Applied Surface Science 553 (2021) 149574

Contents lists available at ScienceDirect

Applied Surface Science

journal homepage: www.elsevier.com/locate/apsusc

Full Length Article

# Structural symmetry evolution in surface and interface of $SrRuO_3$ thin films

Chang Jae Roh [a], Jeong Rae Kim [b,c], Sungjoon Park [b,c,d], Yeong Jae Shin [b,c], Bohm-Jung Yang [b,c,d], Tae Won Noh [b,c], Jong Seok Lee [a,*]

[a] Department of Physics and Photon Science, Gwangju Institute of Science and Technology (GIST), Gwangju 61005, Republic of Korea
[b] Center for Correlated Electron Systems, Institute for Basic Science (IBS), Seoul 08826, Republic of Korea
[c] Department of Physics and Astronomy, Seoul National University (SNU), Seoul 08826, Republic of Korea
[d] Center for Theoretical Physics (CTP), Seoul National University (SNU), Seoul 08826, Republic of Korea

ARTICLE INFO

*Keywords:*
Interface
Surface
Crystallographic symmetry
$SrRuO_3$ thin film
Second harmonic generation

ABSTRACT

Recent advances in thin film technologies enable us to engineer structural details of surface and interface in transition metal oxide films, and provide numerous valuable opportunities to manipulate electric and magnetic properties via strong couplings among charge, spin, and lattice degrees of freedom. In this work, we exploit an optical second harmonic generation technique to determine crystalline symmetries of surface and interface of compressively strained $SrRuO_3$ thin films, which have been widely used as one of representative ferromagnetic metals in oxide devices. We reveal that the structural symmetries of the surface, the inner-bulk part, and the interface of the films are given distinctly owing to the compressive strain and its relaxation. Furthermore, we trace evolutions of the surface/interface structural symmetries with variations of temperature and film thickness, and discuss their similarities and differences compared to the bulk crystal. The structural phase diagram presented here will provide fundamental information of the surface and interface structural symmetry in exploring electronic and magnetic phenomena emerging in relevant oxide heterostructures.

## 1. Introduction

Surface and interface of condensed matters have attracted lots of attentions as the arrangement of the crystalline lattice can be largely altered near the structural boundary. Although the atomic arrangements at surface and interface are usually difficult to control, they can provide unique structural environments to stabilize unconventional electric and magnetic phases which are hard to be realized in the bulk state [1–4]. For the transition metal oxides (TMO), charge and spin degrees of freedom are strongly coupled with the crystalline lattice, and hence the structural engineering particularly at surface and interface has been proven to be a quite useful approach to realize numerous intriguing phenomena, such as metal-insulator transition in the $SrRuO_3$ surface [5], superconductivity at the $LaAlO_3$-$SrTiO_3$ interface [6], ferromagnetic metal phase at the $LaMnO_3$-$SrMnO_3$ interface [7], and so on.

For an in-depth study of these novel electric and magnetic properties, it is essential to make a precise characterization of the crystal structure at surface and interface. There are several powerful techniques available to investigate local crystal structures, such as scanning tunneling microscopy, transmission electron microscopy, and surface x-ray scattering measurements combining the coherent Bragg rod analysis [8], and they have been used to uncover lots of intriguing structural details near surface and interface. For example, an evolution of oxygen octahedral rotation could be traced near the interface of $CaTiO_3$ films grown on various substrates [9], and local strain gradient was revealed at the morphological phase boundary in $BiFeO_3$ thin films [10]. Optical second harmonic generation (SHG) has also played an important role in characterizing the crystal structure. Although the optical wave used usually makes the probing area to be fairly large, the SHG can be one of the most sensitive techniques to explore the macroscopic crystalline symmetry of surface and interface because the broken inversion symmetry at the surface/interface can be a primary source of the SHG process particularly for bulk centrosymmetric materials.

In this work, we characterize the crystal structure of surface and interface of $SrRuO_3$ (SRO) thin films grown on $SrTiO_3$ (STO) substrate by using the optical SHG technique. SRO is one of the most widely investigated TMO systems as having itinerant ferromagnetism [11,12] and being commonly utilized as an electrode in oxide devices [13,14]. Although its bulk property has been heavily understood [11,15–17], surface and interface have been comparatively less investigated

* Corresponding author.
*E-mail address:* jsl@gist.ac.kr (J.S. Lee).

https://doi.org/10.1016/j.apsusc.2021.149574
Received 20 December 2020; Received in revised form 4 March 2021; Accepted 13 March 2021
Available online 19 March 2021

particularly for the thin films. Recently, several research groups have reported the magnetic skyrmion emerging in SRO films not only at their interfaces with heavy-ion $SrIrO_3$ or ferroelectric $BaTiO_3$ but also at the surface of the bare SRO films, and this triggered a large attention for characterizing the structural details of surface and interface of SRO films [18–21]. By monitoring the SHG responses of SRO films with various thicknesses and particularly by varying optical geometries, we could distinguish the surface and interface SHG contributions from inner-bulk part. Based on the distinct anisotropic patterns, we could determine the structural symmetries of each region. Furthermore, we discuss how the surface and interface structural symmetries undergo temperature-dependent changes differently from the inner-bulk phase. Finally, we show that the surface magnetic state is given similarly with the bulk state, and extend our discussion to the emergence of magnetic skyrmion in SRO thin films.

## 2. Experimental sections

### 2.1. Thin film growth

SRO thin films were epitaxially grown on the (0 0 1) STO substrate by a pulsed laser deposition method. For STO substrate (Crystec GmbH), an atomically flat surface was obtained by etching process using buffered hydrofluoric acid and by annealing it for 3 h at 1000 °C in air. During the film growth, a KrF excimer layer (LPXpro 210F, Coherent) was operated with a fluence of 1.5 J/cm$^2$, an oxygen pressure was adjusted as 100 mTorr, and a substrate temperature was set to 700 °C. High quality of the films was confirmed by the x-ray diffraction, and dc-resistivity and magnetization obtained with a temperature variation [22].

### 2.2. Second harmonic generation

For the SHG measurements, the SRO films were shined with femto-second wave pulses (Vitara-T; Coherent) at a wavelength of 800 nm. A repetition rate and time duration are 80 MHz and about 30 fs, respectively. The incidence angle was varied from 0° to 45° to distinguish the electric dipole and electric quadrupole contributions for the tetragonal and orthorhombic point groups. Polarization states of fundamental and second harmonic waves were defined by half wave plate and Glan-Taylor polarizer, respectively. Several optical filters were used to separate the second harmonic wave from the fundamental wave, and the intensity of second harmonic wave was detected by photo-multiplier tube (C8855-01; Hamamatsu Photonics). The sample temperature was controlled using cryogenic system (microstatHe; Oxford) and heating stage (THMS600; Linkam Scientific).

## 3. Results and discussion

### 3.1. Selective probe of interface and surface symmetry by second harmonic generation

To begin with, we explain our strategy to investigate the interface and surface structural symmetry of $SrRuO_3$ films by using the optical SHG technique. The SHG is the lowest order nonlinear optical process, and it is mainly contributed to by the electric dipole (ED) and electric quadrupole (EQ) which is represented as $P_i(2\omega) = \chi^{ED}_{ijk}E_j(\omega)E_k(\omega) + \chi^{EQ}_{ijkl}E_j(\omega)\nabla_k E_l(\omega)$ Electric field of the fundamental wave $\vec{E}(\omega)$ induces a second-order nonlinear polarization $\vec{P}(2\omega)$ oscillating at a doubled frequency, which acts as a source of the second harmonic (SH) wave. Here, $\chi^{ED}_{ijk}$ and $\chi^{EQ}_{ijkl}$ are second-order and third-order nonlinear susceptibility tensor components, respectively, and they are given differently according to the structural symmetry. The intensity of the detected SH wave $I_i(2\omega)$ is in proportion to $|P_i(2\omega)|^2$. It is well known that SRO films epitaxially grown on STO(0 0 1) substrate stabilize tetragonal and distorted orthorhombic (or monoclinic) phases depending on their thickness [15,20,23]. Each phase is distinguished by the oxygen octahedral rotation (OOR) patterns. For the tetragonal phase, the compressive strain stabilizes the OOR pattern of $a^0a^0c^-$ in the Glazer notation with the tetragonal *c*-axis being normal to the in-plane. Note that the Glazer notation describes in-phase (+) or anti-phase (–) rotations of $RuO_6$ octahedra around pseudocubic (pc) axes $[1\,0\,0]_{pc}$, $[0\,1\,0]_{pc}$, and $[0\,0\,1]_{pc}$ [24]. For orthorhombic phase, the OOR pattern is $a^-a^-c^+$, which has an orthorhombic *c*-axis lying on the in-plane. It should be noted that thick SRO films have a non-negligible monoclinic distortion (as depicted in Fig. 3(b)), and hence their symmetry is actually assigned as the point group 2/*m* which refers to the distorted orthorhombic structure throughout this paper. Since both tetragonal (4/*mmm*) and (distorted) orthorhombic (2/*m*) structures are centrosymmetric, the bulk ED contribution is forbidden, and instead the bulk EQ and the surface ED should be considered as the sources of the SHG response. Importantly, the bulk EQ contribution for tetragonal and orthorhombic (monoclinic) symmetries should disappear in the normal incidence geometry because the out-of-plane component of electric-field is essential for the EQ contribution for these symmetry groups [22,25] (Supplementary Information S1). Therefore, we can examine the surface and/or interface state by monitoring the SHG responses in the normal incidence geometry. We can furthermore distinguish the surface and interface contributions by choosing the front- or back-side reflection geometry. It should be noted that the penetration depths of fundamental and SH waves with a wavelength $\lambda = 800$ nm and 400 nm for SRO are about 50 nm and 25 nm, respectively [26]. This clearly limits the probing depth to be about 25 nm. Provided that the film is thicker than this probing depth, the front and back side results reflect the crystalline symmetry near the front surface and the bottom interface facing the substrate, respectively.

Let us first examine the SHG results obtained for the thickest film with a thickness $t = 250$ nm. As schematically shown in Fig. 1(a), the SH wave intensity is monitored with a variation of the sample azimuth ($\phi$) in a normal incidence geometry. Polarization states of fundamental and SH waves are set either in cross (XY) or in parallel (XX) configuration. Fig. 1(b) and (d) compare the SHG anisotropy patterns obtained in the front- and back-side reflection geometries for the XY polarization configuration. Signal amplitudes are similar, but anisotropy appears totally different; a clear two-fold periodicity is observed for the front-side result, but a four-fold periodic pattern appears with a large isotropic contribution for the back-side result. Their clear differences imply that distinct crystalline symmetries are stabilized near the top surface and the bottom interface facing the substrate.

By examining thickness-dependent SHG anisotropies, we can obtain a further insight about the distinct structural symmetries at surface and interface of SRO films. Fig. 2(a) displays SHG anisotropy patterns obtained from the front side with varying the film thickness from 4 nm to 250 nm. The upper and lower panels are results for the XY and XX polarization configurations, respectively. As depicted in Fig. 2(b), the finite penetration depth of fundamental and SH waves allows the probe of only the top surface for the relatively thick films with $t \gtrsim 50$ nm and the probe of both the top surface and the bottom interface for the thinner films. The two-fold anisotropic pattern observed for $t = 250$ nm remains the same for $t = 50$ nm implying that the surface structural symmetry is maintained for the relatively thick films. For the thinnest film with $t = 4$ nm, a four-fold periodic pattern is observed with a non-negligible isotropic contribution. It is worth to note that this behavior is essentially the same with the back side results for $t = 250$ nm (shown in Fig. 1). We therefore consider that the SHG results for the thinnest film are mainly contributed to by the bottom interface facing the STO substrate. Note that the SHG response from the bare STO substrate is negligible since it belongs to centrosymmetric symmetry (cubic point group *m*3*m*). For two intermediate thicknesses, i.e., $t = 10$ and 30 nm, the SHG anisotropy patterns appear more complicated. In these cases, the films are thin enough so that not only the top surface but also the

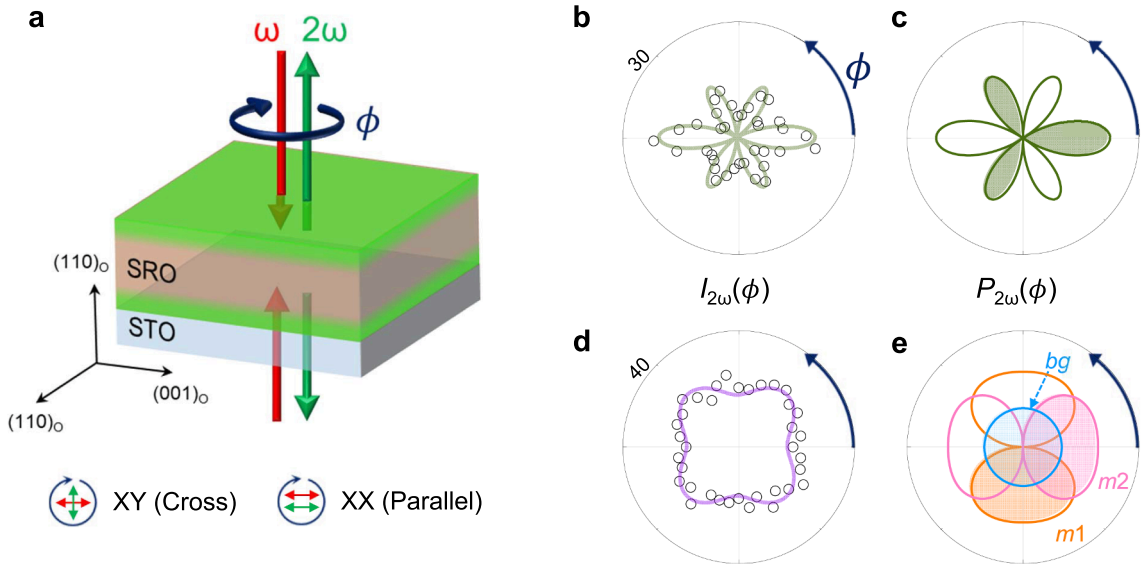


**Fig. 1.** Symmetry characterization of surface and interface of the 250 nm thick $SrRuO_3$ (SRO) film by optical second harmonic generation (SHG). a) Schematic description of normal incident geometry and polarization states of fundamental (red) and SHG (green) waves. Backward reflection geometry is taken from the front and back side of the film to probe the front surface and bottom interface of the film, respectively. b, d) Azimuth angle dependent SHG intensity obtained from the front side (b) and the back side (d). Fitting results are shown with solid lines. c, e) Second order nonlinear polarization $\boldsymbol{P}_{2\omega}(\boldsymbol{\phi})$ constituting each fitting curve for the front side (c) and back side (e) results. Filled and empty parts indicate positive and negative phases, respectively, of $\boldsymbol{P}_{2\omega}(\boldsymbol{\phi})$. A successful fitting for the back side result requires multiple contributions, namely, contributions from two monoclinic domains ($m1$ and $m2$) and an isotropic background (bg).

bottom interface can contribute to the SHG response in the front side reflection geometry. Actually, they have both isotropic and two-fold anisotropy which are features of the films with $t = 4$ nm and $t \gtrsim 50$ nm, respectively. It should be also noted that the $t = 10$ nm film has fairly large SHG intensity. This implies that the polar structural distortion should be large in these films with an intermediate thickness; a competition between the strained tetragonal phase and the bulk-like distorted orthorhombic phase may lead to the structural phase with a larger structural distortion [22].

### 3.2. Characterization of interface and surface structure from the symmetry analyses

We determine the structural symmetries of surface and interface by fitting the anisotropy patterns of the SHG intensity presented in Figs. 1 and 2. Let us first examine the symmetry of the surface. For the thick SRO films, their structural symmetry is often assigned to be the orthorhombic phase (Fig. 3 (a)), but it is actually accompanied by the non-negligible monoclinic distortion as depicted in Fig. 3(b); orthorhombic axes $a_o$ ($[100]_o$) and $b_o$ ($[010]_o$) lie along $[1\bar{1}0]_{pc}$ and $[110]_{pc}$, respectively, but their angle is slightly deviated from 90.0° of the ideal orthorhombic phase as about 89.4° [27]. Hence the symmetry of the thick film is assigned to be point group $2/m$. At the film surface, a structural discontinuity removes the two-fold rotation symmetry operation, and accordingly the structural symmetry should become the monoclinic point group $m$. We actually confirm that the ED contribution from the point group $m$ can successfully explain the front-side results for $t = 250$ nm; solid line in Fig. 1(b) (and 2(a)-rightmost) is the fitting curve obtained from the azimuth-dependence of second-order polarization $P_{2\omega}(\phi)$ shown in Fig. 1(c). Note that analytic forms of the azimuth dependent SHG intensity used for the fit analyses are given in Supplementary Information S2 for monoclinic (2 and $m$) and triclinic (1) point groups. For the thin SRO films with, e.g., $t = 4$ nm, we previously characterized the point group of its inner-bulk part as $4/m$ by monitoring the SHG intensity in the grazing incidence [22]. Accordingly, their surface crystalline symmetry should be point group 4. Note that this symmetry does not allow any in-plane polarization component in the SH wave. Although the 4 nm thick film exhibits characteristic anisotropy pattern (Fig. 2(a)), it resembles the response for the 250 nm thick film obtained from the back side. We therefore consider that the SHG response from the front surface for $t = 4$ nm should be negligible. This leads us to conclude that the surface of the SRO films facing the air is characterized to have the point group 4 and $m$ for the thin ($t \sim 4$ nm) and thick ($t \gtrsim 50$ nm) films, respectively.

We now turn our discussion to the structural symmetry of the SRO interface facing the STO substrate. Considering the distinct SHG anisotropy patterns obtained for the front-side and back-side reflection geometries (Fig. 1), it is clear that the crystalline symmetry near the bottom interface should be different from the top surface of the film. As a compressive strain stabilizes the centrosymmetric tetragonal phase $4/m$ near the substrate, one may consider the point group 4 as the symmetry of its interface. As aforementioned, this symmetry does not allow any ED SHG contribution in the normal incidence geometry. Therefore, the observed SHG anisotropy strongly suggests that an additional symmetry lowering, differently from the symmetry 4, should occur near the SRO-STO interface. Importantly, the four-fold-like anisotropy pattern cannot be attributable simply to any single structural phase since the four-fold contribution for SHG process, if it would exist, is strongly coupled with two-fold and six-fold contributions (Supplementary Information S2). Instead, we can easily reproduce such feature by considering multiple contributions from the monoclinic domains with different mirror planes. We consider contributions from two monoclinic domains ($m1$ and $m2$) and a finite background ($bg$) as depicted in Fig. 1(e), and can fit the experimental result successfully from their incoherent summation as $I_{2\omega}(\phi) \sum_i \left[P^i_{2\omega}(\phi)\right]^2$ with $i = m1$, $m2$ and $bg$.

Actually, it is not straightforward to conceive the monoclinic symmetry via an additional symmetry lowering from the $4/m$ symmetry of the inner part of SRO films. Although the in-plane lattice of the thin SRO films is fully clamped to that of the STO substrate, the oxygen octahedron rotation patterns for the tetragonal SRO are given distinctly; STO has no OOR ($a^0a^0a^0$), but tetragonal SRO has an out-of-phase rotation of $RuO_6$ octahedra along the out-of-plane direction ($a^0a^0c^-$). Therefore, there should be a relaxation of the OOR pattern through few- or several unit cells near the SRO-STO interface [28–30]. As demonstrated in the

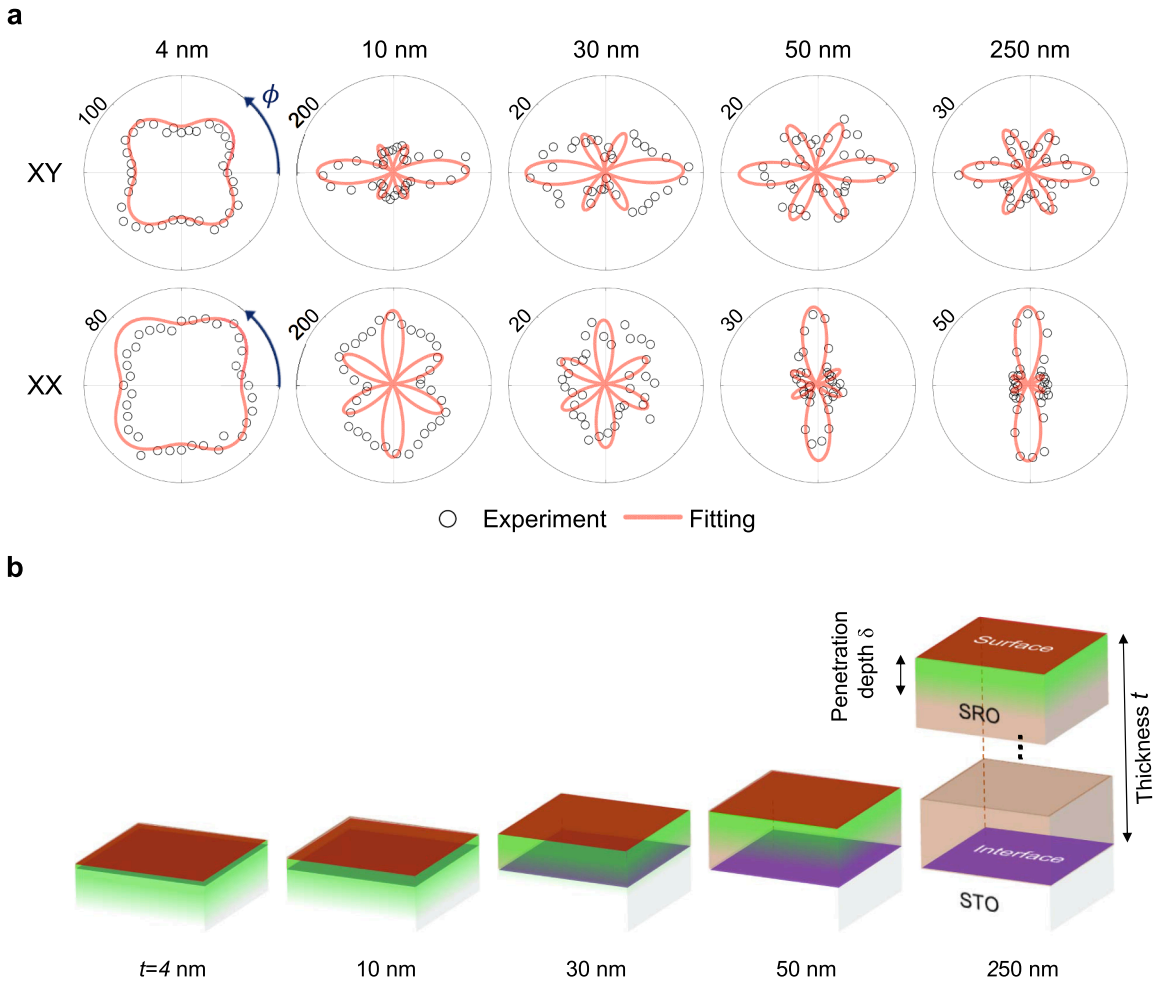


**Fig. 2.** SHG results of $SrRuO_3$ thin films with a thickness $t = 4$, 10, 30, 50, and 250 nm. a) Azimuth angle-dependent SHG intensity monitored for XY (upper) and XX (lower) polarization configurations. The symbol and solid line stand for the monitored intensity and fitting results, respectively. For $t = 4$ nm, two monoclinic domains formed at the interface are considered similarly for the bottom interface contribution for $t = 250$ nm shown in Fig. 1. For $t = 10$–250 nm, a single monoclinic phase formed at the surface is considered. For $t = 10$ nm, the fitting quality is less satisfying compared to other results, and it can be improved by considering contributions from both top surface and bottom interface (see Supplementary Information S2). b) Schematic description of the penetration depth (marked with green color) for each film.

Supplementary Information S4, the asymmetric formation of the oxygen atoms removes the mirror plane along the in-plane direction so that the point group for this region is defined as 4. Therefore, it is not possible to have the point group *m* even from the simple rearrangement of the OOR pattern at the interface. Actually, it is important to note that the mirror plane in the interface point group *m* is lying along the out-of-plane direction, and this symmetry operation does not belong to the point group 4/*m* of the inner part. In this respect, the interface does not share the symmetry operation other than the identity with the inner-bulk part having the point group 4/*m*. Recently, Sohn *et al.* performed the x-ray diffraction study combined with Coherent Bragg rod analysis (COBRA) on SRO films grown on the STO substrate, and revealed large deviations of the crystalline structures near the interface from ideal tetragonal and orthorhombic phases [31]. We conjecture that an additional structural reconstruction may arise from the structural misfits in both the lattice constant and the OOR pattern across the interface as well as from a possible off-stoichiometry [23,31]. Furthermore, the layer-by-layer growth of the initial stage allows to form crystallographic domains with different mirror planes (Fig. 3(c))[32]. In the inner-bulk part of the films, the step-flow growth mode favors a single domain formation, but the strain relaxation may be accompanied by a formation of defect-like states [33], which may be hard to be detected in the present macroscopic measurement.

### 3.3. Temperature-dependent evolution of interface and surface structural symmetry

From these analyses, we could obtain a deep understanding about the crystalline symmetries of the top surface and the bottom interface of the SRO films which turn out to be in the monoclinic or tetragonal phases. For the bulk SRO, the orthorhombic crystalline structure undergoes a transition to the tetragonal structure at 820 K [11]. Similar structural changes are revealed in thin SRO films whereas the transition temperature is lowered to about 550 K due to the strain [15,17]. In this respect, it is worthwhile to examine how the crystalline symmetries of surface and interface of SRO films vary as a function of temperature. Fig. 4(a) shows representative SHG anisotropy results for $t = 250$ nm obtained at 80 K, 300 K, and 573 K. As temperature decreases down to 80 K, the SHG polar pattern remains as being two-fold periodic whereas the overall intensity becomes stronger. On the other hand, the SHG intensity becomes diminished with an increase of temperature to 573 K. We integrate the SHG intensity over the full range of the sample azimuth, and present its temperature dependence in Fig. 4(b) for all the films investigated. The SHG intensity decreases as temperature increases, and becomes negligible at about 500 K. This clearly indicates that the crystalline structure of surface or interface undergoes a transition to different states at high temperature. Considering that the inner-

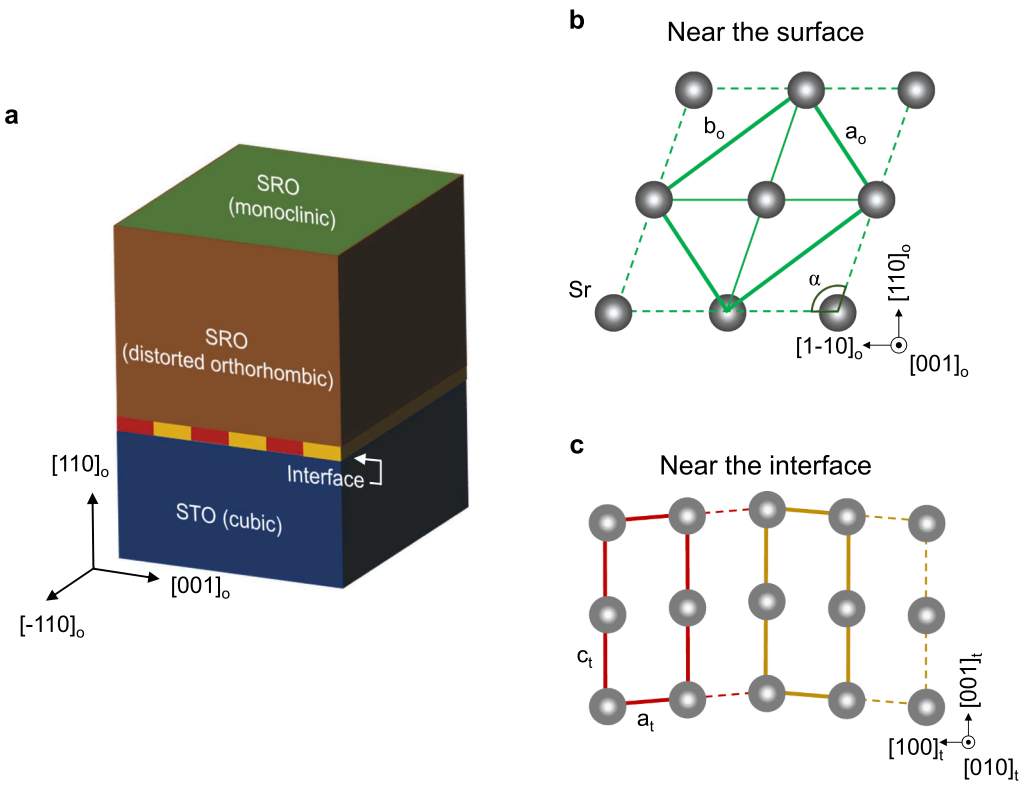


**Fig. 3.** Crystal structures of surface, inner-bulk, and interface for $SrRuO_3$ (SRO) films grown on $SrTiO_3$ (STO) substrate. a) Cross-sectional view of the crystal structures of the SRO film on STO. For the films with a thickness larger than 50 nm, the inner-bulk part is dominated by the distorted orthorhombic or the monoclinic (2/*m*) phase. Accordingly, its surface should have the monoclinic symmetry *m*. And, the interface facing the substrate is characterized as the multi-domain state with a monoclinic point group *m*. b,c) Atomic arrangements for the monoclinic symmetry of surface (b) and interface (c) of SRO films. Crystallographic orientations are given in the orthorhombic and tetragonal conventions for (b) and (c), respectively. In (b), a monoclinic distortion is indicated with α deviating from 90°. Note that the interface is depicted to have the multi-domain phase (a and c).

bulk part of the SRO films undergoes the structural transition to the higher symmetry, i.e., the tetragonal structure with 4/*mmm* around 600 K [15,17], we consider 4 *mm* or 4 as the surface symmetry at the high temperature. Since both symmetries do not contribute to the SHG response in the normal incidence, we can consistently understand the diminished SHG response at the high temperature in terms of the corresponding structural change of the surface. It should be noted that this high-temperature structural phase should be common for all the SRO films since both the grazing-incidence and normal-incidence SHG intensities, which are sensitive to the bulk and surface/interface symmetries, respectively, become negligible at the high temperature irrespective of the film thickness [15,17,34].

We present in Fig. 4(d) the structural phase diagram of the surface, the interface, and (inner-) bulk of SRO films grown on the STO substrate with variations of temperature and the film thickness. Whereas surface and interface structures are characterized by the normal-incidence SHG results, structural information for the inner-bulk is taken from the grazing-incidence SHG result (Fig. 4(c)) and also from previous x-ray diffraction study [17]. As temperature increases, the higher structural symmetries are preferred for both the bulk and interface/surface. By the way, it is worthwhile to point out three characteristic features of structural changes for surface and interface of SRO films. First, the transition temperature for the surface structure particularly of the thick films is noticeably lower than that for the inner-bulk part of the film. As shown in Fig. 4(c), although the inner-bulk phase for $t = 250$ nm undergoes the transition at about 550 K [17], which is manifested by the grazing-incidence SHG result, our normal-incidence SHG results imply that the surface structure changes into the high symmetry phase already at about 450 K. Since the surface structure is naturally connected to the crystalline network of the inner-bulk part, such a large difference in the temperature of the structural changes is rather unexpected. Further investigations are desired to elucidate this observation by considering cooperative effects of a dimensionality difference between the inner-bulk and the surface, atomic defects including oxygen vacancy [35–37], and so on. Second, as the film becomes thinner to, e.g., $t = 50$ nm, the transition temperature for the surface symmetry increases slightly, and it becomes comparable to that of the inner-bulk part. We consider that the larger strain effect for the thinner film would influence the entire area of the film, and hence the surface and inner-bulk part undergo the structural change at the similar temperature. Another interesting aspect can be pointed out for the interface state of the thin films. Differently from the surface (for $t \geq 50$ nm), the interface SHG response (for $t \leq 30$ nm) shows a much gradual $T$-dependent reduction (Fig. 4(b)). We conjecture that the evolution of the structural change near the interface would be impeded by the stronger strain effect by the substrate as well as the existence of the multi-domain states formed near the interface.

### 3.4. Discussion about magnetic properties of the $SrRuO_3$ film surface

Finally, we discuss the interface/surface magnetic properties based on our SHG results. As shown in Fig. 4(b), SHG intensity increases at about 150 K with a decrease of temperature, and this is reminiscent of the ferromagnetic transition for the SRO films. This strongly suggests that the surface/interface of the SRO film is compatible with the ferromagnetic spin order [38,39] Ferromagnetic transition temperature of the surface/interface is also included in the phase diagram shown in Fig. 4(d). The magnetic transition temperature does not show a noticeable change with varying the film thickness, suggesting that the ferromagnetic order is relatively less influenced by the details of the crystalline structure.

From this information about the ferromagnetic surface state together with the surface structural symmetry, it is worthy of discussing the possible formation of a magnetic skyrmion near the SRO film surface. Recently, the magnetic skyrmion was intensively discussed in SRO films [18–20,31], and it emerges from the Dzyaloshinskii-Moriya (DM) interaction for otherwise ferromagnetically ordered spins. According to the Moriya's rule, the DM vectors for the 4 *mm* surface/interface are defined to lie in the plane as being cyclic in the same sense [40]. This is the case for the thin films with, e.g., $t = 4$ nm where the skyrmion is

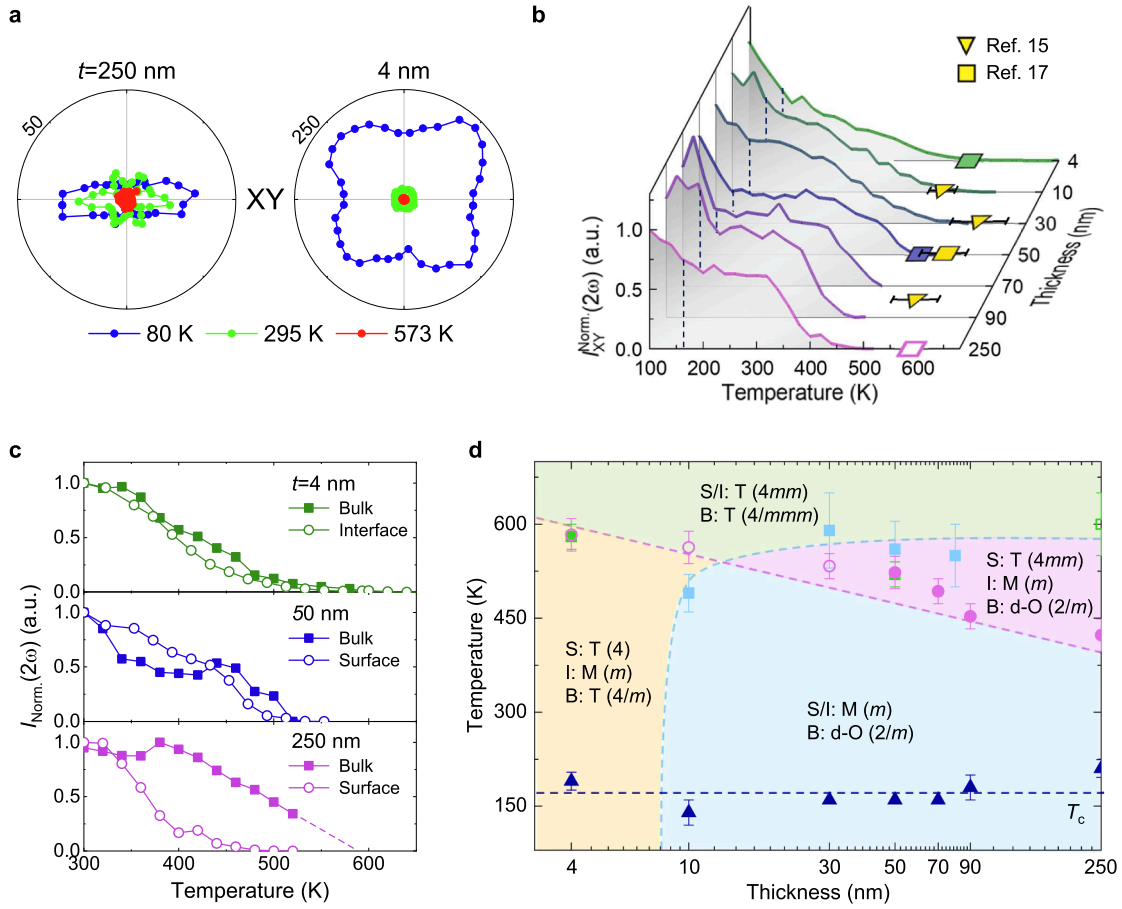


**Fig. 4.** Temperature-dependent SHG results for $SrRuO_3$ films and structural phase diagram. a) Azimuth angle-dependent SHG intensity monitored at 80 K (blue), 300 K (green), and 573 K (red) for the film thickness $t = 250$ nm and 4 nm. b) Temperature-dependent integrated SHG intensity for the XY configuration. Symbols indicate the structural transition temperatures for the inner-bulk of $SrRuO_3$ films with corresponding thicknesses. Symbols of yellow color are taken from the x-ray diffraction studies (Refs. [15;17]), and symbols of other colors are taken from the grazing-incidence SHG results (Fig. 4(c)). Dashed lines correspond to the ferromagnetic transition temperature ~160 K. c) Temperature-dependent SHG intensities representing the surface/interface symmetry (open) and the inner-bulk symmetry (filled), which are taken from the normal incidence and grazing incidence geometry, respectively. d) Structural phase diagram of surface (S, filled pink circle), interface (I, empty pink circle) and bulk (B, light blue square) of $SrRuO_3$ films. Tetragonal, monoclinic, and distorted orthorhombic structures are abbreviated by T, M, and d-O, respectively. Dashed lines are guide to the eyes to distinguish different crystallographic phases. Surface ferromagnetic transition temperature ($T_c$) is given with a triangle which appears almost independently of the film thickness.

possible formed. For the surface of thicker SRO films ($t \geq 50$ nm), the symmetry is characterized as the monoclinic point group *m* differently from 4 or 4 *mm* for surfaces of thinner films. In this case of the monoclinic point group *m*, the directions of DM vectors are not fixed by the symmetry alone, and the formation of skyrmion is less preferred (Supplementary Information S5). It should be also noted that inner-bulk of the films maintain the inversion symmetry which forbids DM interaction and hence the collinear ferromagnetic order is favored. Therefore, even if the surface/interface favors formation of skyrmion, there will be energy penalization from the bulk for forming skyrmion as the thickness increases. By considering structural symmetries of the surface and the inner-bulk of SRO films, the skyrmion can be stabilized in thin films with the thickness less than 10 nm, and it will be less favored with an increase of the film thickness [20].

## 4. Conclusion

In summary, we investigated the crystallographic symmetry of surface and interface for the compressively strained $SrRuO_3$ thin films grown on $SrTiO_3$ (0 0 1) substrate by using the optical second harmonic generation technique. By adjusting optical configurations as well as the film thickness, we could successfully distinguish the SHG contributions from the surface, the inner-bulk, and the interface facing the substrate. As a result, we characterized the surface of SRO films to have the tetragonal or monoclinic symmetry depending on the film thickness, and the interface facing the $SrTiO_3$ substrate to have the monoclinic symmetry possibly due to the structural reconstruction at the interface. Moreover, we demonstrated that all the parts of the surface, the inner-bulk, and the interface undergo structural transitions with an increase of temperature, and each exhibits distinct temperature-dependent behaviors which are attributable to the characteristic structural environments of each area. In these respects, our work provides useful information about the structural details of surface and interface which is crucial in exploiting $SrRuO_3$ thin films for the oxides devices. Furthermore, we anticipate that our work can be a valuable guideline in exploiting transition metal oxide heterostructures where the interface structure should be carefully engineered for both electronic and spintronic applications.

## CRediT authorship contribution statement

**Chang Jae Roh:** Conceptualization, Methodology, Investigation, Formal analysis, Data curation, Validation, Visualization, Writing - original draft, Writing - review & editing. **Jeong Rae Kim:** Resources,

Validation. **Sungjoon Park:** Formal analysis, Writing - original draft. **Yeong Jae Shin:** Resources. **Bohm-Jung Yang:** Formal analysis, Funding acquisition. **Tae Won Noh:** Resources, Funding acquisition. **Jong Seok Lee:** Conceptualization, Supervision, Project administration, Visualization, Writing - original draft, Writing - review & editing, Funding acquisition.

## Declaration of Competing Interest

The authors declare that they have no known competing financial interests or personal relationships that could have appeared to influence the work reported in this paper.

## Acknowledgements

C.J. Roh and J.S. Lee were supported by the Ministry of Science, ICT and Future Planning (Nos. 2015R1A5A1009962, 2018R1A2B2005331). J.R. Kim, Y.J. Shin, and T.W. Noh were supported by IBS-R009-D1. S. P. and B.J.Y. were supported by the Institute for Basic Science in Korea (Grant No. IBS-R009-D1), Samsung Science and Technology Foundation under Project Number SSTF-BA2002-06, Basic Science Research Program through the National Research Foundation of Korea (NRF) (Grant No. 0426-20200003), and the U.S. Army Research Office and and Asian Office of Aerospace Research & Development (AOARD) under Grant Number W911NF-18-1-0137. We also acknowledge the computational support and invaluable discussions from D.G. Jeong, H.I. Ju, H.J. Oh, E. K. Ko, and H.G. Lee.

## Appendix A. Supplementary material

Supplementary data to this article can be found online at https://doi.org/10.1016/j.apsusc.2021.149574.

## References

[1] A. Soumyanarayanan, N. Reyren, A. Fert, C. Panagopoulos, Emergent phenomena induced by spin–orbit coupling at surfaces and interfaces, Nature 539 (2016) 509.
[2] A. Bhattacharya, S.J. May, Magnetic Oxide Heterostructures, Annu. Rev. Mater. Res. 44 (2014) 65–95.
[3] Mariola O. Ramirez, Tom T.A. Lummen, Irene Carrasco, Eftihia Barnes, Ulrich Aschauer, Dagmara Stefanska, Arnab Sen Gupta, Carmen de las Heras, Hirofumi Akamatsu, Martin Holt, Pablo Molina, Andrew Barnes, Ryan C. Haislmaier, Przemyslaw J. Deren, Carlos Prieto, Luisa E. Bausa, Nicola A. Spaldin, Venkatraman Gopalan, Emergent room temperature polar phase in CaTiO3 nanoparticles and single crystals, APL Mater. 7 (2019) 011103.
[4] P. Yu, Y.-H. Chu, R. Ramesh, Oxide interfaces: pathways to novel phenomena, Mater. Today 15 (2012) 320–327.
[5] Han Gyeol Lee, Lingfei Wang, Liang Si, Xiaoyue He, Daniel G. Porter, Jeong Rae Kim, Eun Kyo Ko, Jinkwon Kim, Sung Min Park, Bongju Kim, Andrew Thye Shen Wee, Alessandro Bombardi, Zhicheng Zhong, Tae Won Noh, Atomic-Scale Metal–Insulator Transition in SrRuO3 Ultrathin Films Triggered by Surface Termination Conversion, Adv. Mater. 32 (2019) 1905815.
[6] C. Richter, H. Boschker, W. Dietsche, E. Fillis-Tsirakis, R. Jany, F. Loder, L. F. Kourkoutis, D.A. Muller, J.R. Kirtley, C.W. Schneider, J. Mannhart, Interface superconductor with gap behaviour like a high-temperature superconductor, Nature 502 (2013) 528–531.
[7] M. Hiroyuki Yamada, Kawasaki, $LaMnO_3/SrMnO_3$ interfaces with coupled charge-spin-orbital modulation, Appl. Phys. Lett. 89 (2006), 052506.
[8] D.P. Kumah, A. Malashevich, A.S. Disa, D.A. Arena, F.J. Walker, S. Ismail-Beigi, C. H. Ahn, Effect of Surface Termination on the Electronic Properties of $LaNiO_3$ Films, Phys. Rev. Appl 2 (2014), 054004.
[9] Y. Yuan, L.u. Yanfu, G. Stone, K.e. Wang, C.M. Brooks, D.G. Schlom, S.B. Sinnott, H. a. Zhou, V. Gopalan, Three-dimensional atomic scale electron density reconstruction of octahedral tilt epitaxy in functional perovskites, Nat. Commun. 9 (2018) 5220.
[10] Kanghyun Chu, Byung-Kweon Jang, Ji Ho Sung, Yoon Ah Shin, Eui-Sup Lee, Kyung Song, Jin Hong Lee, Chang-Su Woo, Seung Jin Kim, Si-Young Choi, Tae Yeong Koo, Yong-Hyun Kim, Sang-Ho Oh, Moon-Ho Jo, Chan-Ho Yang, Enhancement of the anisotropic photocurrent in ferroelectric oxides by strain gradients, Nat. Nanotechnol. 10 (2015) 972–979.
[11] G. Koster, L. Klein, W. Siemons, G. Rijnders, J.S. Dodge, C.-B. Eom, D.H.A. Blank, M.R. Beasley, Structure, physical properties, and applications of $SrRuO_3$ thin films, Rev. Mod. Phys. 84 (2012) 253.
[12] Y.J. Chang, C.H. Kim, S.-H. Phark, Y.S. Kim, J. Yu, T.W. Noh, Fundamental Thickness Limit of Itinerant Ferromagnetic $SrRuO_3$ Thin Films, Phys. Rev. Lett. 103 (2009), 057201.
[13] W. Ratcliff II, V. Zahra Yamani, T.R. Anbusathaiah, P.A. Gao, H. Kienzle, I.T. Cao, Electric-field-controlled antiferromagnetic domains in epitaxial $BiFeO_3$ thin films probed by neutron diffraction, Phys. Rev. B 87 (2013) 140405(R).
[14] E. Arenholz, G. van der Laan, A. Fraile-Rodríguez, P. Yu, Q. He, R. Ramesh, Probing ferroelectricity in $PbZr_{0.2}Ti_{0.8}O_3$ with polarized soft x rays, Phys. Rev. B 82 (2010) 140103(R).
[15] S.H. Chang, Y.J. Chang, S.Y. Jang, D.W. Jeong, C.U. Jung, Y.-J. Kim, J.-S. Chung, T. W. Noh, Thickness-dependent structural phase transition of strained $SrRuO_3$ ultrathin films: The role of octahedral tilt, Phys. Rev. B 84 (2011), 104101.
[16] D. Kan, R. Aso, H. Kurata, Y. Shimakawa, Thickness-Dependent Structure-Property Relationships in Strained (110) $SrRuO_3$ Thin Films, Adv. Funct. Mater. 23 (2013) 1129–1136.
[17] K.J. Choi, S.H. Baek, H.W. Jang, L.J. Belenky, M. Lyubchenko, C.-B. Eom, Phase-Transition Temperatures of Strained Single-Crystal $SrRuO_3$ Thin Films, Adv. Mater. 22 (2010) 759–762.
[18] J. Matsuno, N. Ogawa, K. Yasuda, F. Kagawa, W. Koshibae, N. Nagaosa, Y. Tokura, M. Kawasaki, Interface-driven topological Hall effect in $SrRuO_3$-$SrIrO_3$ bilayer, Sci. Adv. 2 (2016), e1600304.
[19] Lingfei Wang, Qiyuan Feng, Yoonkoo Kim, Rokyeon Kim, Ki Hoon Lee, Shawn D. Pollard, Yeong Jae Shin, Haibiao Zhou, Wei Peng, Daesu Lee, Wenjie Meng, Hyunsoo Yang, Jung Hoon Han, Miyoung Kim, Qingyou Lu, Tae Won Noh, Ferroelectrically tunable magnetic skyrmions in ultrathin oxide heterostructures, Nat. Mater. 17 (2018) 1087–1094.
[20] Q. Qin, L. Liu, W. Lin, X. Shu, Q. Xie, Z. Lim, C. Li, S. He, G.M. Chow, J. Chen, Emergence of Topological Hall Effect in a $SrRuO_3$ Single Layer, Adv. Mater. 31 (2019) 1807008.
[21] C. Wang, C.-H. Chang, A. Herklotz, C. Chen, F. Ganss, U. Kentsch, D. Chen, X. Gao, Y.-J. Zeng, O. Hellwig, M. Helm, S. Gemming, Y.-H. Chu, S. Zhou, Topological Hall Effect in Single Thick $SrRuO_3$ Layers Induced by Defect Engineering, Adv. Electron. Mater. 6 (2020) 2000184.
[22] Chang Jae Roh, Myung-Chul Jung, Jeong Rae Kim, Kyoung-June Go, Jinkwon Kim, Ho Jun Oh, Young-Ryun Jo, Yeong Jae Shin, Jeong Gi Choi, Bong-Joong Kim, Q1 Do Young Noh, Si-Young Choi, Tae Won Noh, Myung Joon Han, Jong Seok Lee, Polar Metal Phase Induced by Oxygen Octahedral Network Relaxation in Oxide Thin Films, Small 16 (2020) 2003055.
[23] R. Gao, Y. Dong, H. Xu, H. Zhou, Y. Yuan, V. Gopalan, C. Gao, D.D. Fong, C. T. Chen, Z. Luo, L.W. Martin, Interfacial Octahedral Rotation Mismatch Control of the Symmetry and Properties of $SrRuO_3$, ACS Appl. Mater. Interfaces 8 (2016) 14871–14878.
[24] A.M. Glazer, The Classification of Tilted Octahedra in Perovskites, Acta Crystallogr. B 28 (1972) 3384.
[25] D.H. Torchinsky, H. Chu, L. Zhao, N.B. Perkins, Y. Sizyuk, T. Qi, G. Cao, D. Hsieh, Structural Distortion-Induced Magnetoelastic Locking in $Sr_2IrO_4$ Revealed through Nonlinear Optical Harmonic Generation, Phys. Rev. Lett. 114 (2015), 096404.
[26] R.B. Wilson, B.A. Apgar, L.W. Martin, D.G. Cahill, Thermoreflectance of metal transducers for optical pump-probe studies of thermal properties, Opt. Express 20 (2012) 28829–28838.
[27] A. Vailionis, W. Siemons, G. Koster, Room temperature epitaxial stabilization of a tetragonal phase in $ARuO_3$ (A=Ca and Sr) thin films, Appl. Phys. Lett. 93 (2008), 051909.
[28] R. Aso, D. Kan, Y. Shimakawa, H. Kurata, Atomic level observation of octahedral distortions at the perovskite oxide heterointerface, Sci. Rep. 3 (2013) 2214.
[29] D. Kan, M. Anada, Y. Wakabayashi, H. Tajiri, Y. Shimakawa, Oxygen octahedral distortions in compressively strained $SrRuO_3$ epitaxial thin films, J. Appl. Phys. 123 (2018), 235303.
[30] Seung Gyo Jeong, Gyeongtak Han, Sehwan Song, Taewon Min, Ahmed Yousef Mohamed, Sungkyun Park, Jaekwang Lee, Hu Young Jeong, Young-Min Kim, Deok-Yong Cho, Woo Seok Choi, Propagation Control of Octahedral Tilt in SrRuO3 via Artificial Heterostructuring, Adv. Sci. 7 (2020) 2001643.
[31] Byungmin Sohn, Bongju Kim, Se Young Park, Hwan Young Choi, Jae Young Moon, Taeyang Choi, Young Jai Choi, Tae Won Noh, Hua Zhou, Seo Hyoung Chang, Jung Hoon Han, Changyoung Kim, Emergence of robust 2D skyrmions in SrRuO3 ultrathin film without the capping layer, Preprint at https://arxiv.org/abs/1810.01615 (2018).
[32] J. Choi, C.B. Eom, G. Rijnders, H. Rogalla, D.H.A. Blank, Growth mode transition from layer by layer to step flow during the growth of heteroepitaxial $SrRuO_3$ on (001) $SrTiO_3$, Appl. Phys. Lett. 19 (2001) 1447.
[33] C. Ghica, R.F. Negrea, L.C. Nistor, C.F. Chirila, L. Pintilie, Nanoscale monoclinic domains in epitaxial $SrRuO_3$ thin films deposited by pulsed laser deposition, J. Appl. Phys. 116 (2014), 023516.
[34] A. Vailionis, W. Siemons, G. Koster, Strain-induced single-domain growth of epitaxial $SrRuO_3$ layers on $SrTiO_3$: A high-temperature x-ray diffraction study, Appl. Phys. Lett. 91 (2007), 071907.
[35] L.u. Wenlai, P. Yang, Wen Dong Song, Gan Moog Chow, Jing Sheng Chen, Control of oxygen octahedral rotations and physical properties in $SrRuO_3$ films, Phys. Rev. B 88 (2013), 214115.
[36] J. Shin, A.Y. Borisevich, V. Meunier, E. Jing Zhou, W. Plummer, S.V. Kalinin, A. P. Baddorf, Oxygen-Induced Surface Reconstruction of $SrRuO_3$ and Its Effect on the $BaTiO_3$ Interface, ACS Nano 4 (2010) 4190–4196.
[37] Henning Schraknepper, Christoph Baumer, Regina Dittmann, Roger A. De Souza, Complex behaviour of vacancy point-defects in SrRuO3 thin films, Phys. Chem. Chem. Phys. 17 (2015) 1060.

[38] Y. Ogawa, Y. Kaneko, J.P. He, X.Z. Yu, T. Arima, Y. Tokura, Magnetization-Induced Second Harmonic Generation in a Polar Ferromagnet, Phys. Rev. Lett. 92 (2004), 047401.
[39] Y. Krockenberger, J.S. Lee, D. Okuyama, H. Nakao, Y. Murakami, M. Kawasaki, Y. Tokura, Garnet superlattice as a transparent above-room-temperature polar magnet, Phys. Rev. B 83 (2011), 214414.
[40] A. Crépieux, C. Lacroix, Dzyaloshinsky-Moriya interactions induced by symmetry breaking at a surface, J. Magn. Magn. Mater. 182 (1998) 341–349.